Isomers of SO_3: Infrared absorption of OSOO in solid argon

Shen-Horng Jou, Min-yi Shen, Chin-hui Yu, and Yuan-Pern Lee[a)]
Department of Chemistry, National Tsing Hua University, 101, Sec. 2, Kuang Fu Road, Hsinchu, Taiwan 30043, Republic of China

(Received 5 December 1995; accepted 3 January 1996)

Sulfur trioxide (SO_3) isolated in solid argon at 12 K was irradiated with light at 193 nm from an ArF excimer laser. Recombination of photofragments O and SO_2 produces OSOO that absorbs at 1229.6, 1041.3, and 597.6 cm^{-1}. The assignments are based on observed ^{34}S- and ^{18}O-isotopic shifts. Theoretical calculations using the B-P86 and the B3-LYP density functional methods were carried out for five isomers of SO_3; energies and vibrational wave numbers were predicted for each one. Observed line positions, infrared intensities, and isotopic shifts fit well with those predicted for *cis*-OSOO at the B-P86 level. Further irradiation of the matrix sample with emission at 248 nm from a KrF laser bleached OSOO and enhanced absorption lines of SO_2 and, to a lesser extent, of SO_3. The mechanism of formation of OSOO in a matrix cage is discussed. © *1996 American Institute of Physics.* [S0021-9606(96)00214-3]

I. INTRODUCTION

Sulfuric acid is a primary constituent of acid rain.[1,2] It also plays an important role in the formation of atmospheric aerosols; consequently it influences the climate and the depletion of ozone.[3,4] The major channel for the formation of sulfuric acid from sulfur compounds involves oxidation of SO_2. The process,[5,6]

$$SO_2+OH+M\rightarrow HOSO_2+M, \quad (1)$$

$$HOSO_2+O_2\rightarrow HO_2+SO_3, \quad (2)$$

$$SO_3+H_2O\rightarrow H_2SO_4, \quad (3)$$

is generally accepted to be responsible for homogeneous oxidation of SO_2 in the atmosphere. Hence, sulfur trioxide (SO_3) is an important intermediate in the oxidation processes of sulfur compounds.

Vibrational spectra of SO_3 either in the gaseous phase or isolated in a matrix were reported by numerous investigators;[7–14] they are consistent with the well established planar structure of D_{3h} symmetry. Formation of isomers of SO_3 may be suspected, especially at low temperature, but such isomers remain uncharacterized, either theoretically or experimentally. A few matrix-isolation experiments relevant to formation of SO_3 and perhaps its isomers were reported. Hopkins *et al.*[15] measured IR and Raman spectra of low-temperature condensates of SO_2 subjected to radio-frequency and microwave discharges; they observed production of SO_3, S_2O, S_3, S_4, O_3, and a poly (sulfur oxide). Kugel and Taube[16] photolyzed matrix samples containing O_3 and SO_3; they observed new IR absorption lines attributed to SO_4 from reaction of SO_3 and O. Formation of OSOO from reaction of SO_3 with O in matrices was also suspected, but no experimental evidence was obtained. Sodeau and Lee[17] photolyzed matrix samples (Ar, N_2, or O_2) containing SO_2 with either a 1000 W Hg arc or a 20 W Zn lamp; they found that monomeric SO_2 was inert, whereas the dimeric species was readily photooxidized to SO_3 in an O_2 matrix at 12 K.

We demonstrated previously that during photolysis of a matrix sample the matrix cage effect provides excellent opportunities for photofragments to recombine to form various isomers of parent molecules that may be difficult to prepare in the gaseous phase.[18–20] We produced and identified *cis–cis* and *trans-perp* HOONO by irradiation of nitric acid ($HONO_2$) isolated in solid Ar at low temperature with a 193-nm excimer laser.[18] In the present work with a similar technique we irradiated samples of matrix-isolated sulfur trioxide (SO_3) to observed infrared absorption lines due to OSOO. With the first identification of this isomer of SO_3, we expect that its role in atmospheric chemistry will be determined in due course.

II. EXPERIMENTS

The experimental setup is similar to that described previously.[18,21] The cold matrix support at 13 K was a copper mirror gold-plated to reflect the IR beam to the detector. Matrix-isolated samples were prepared by passing a stream of Ar over a glass trap containing SO_3 and H_2SO_4; the trap was cooled to approximately 210 K to reduce the vapor pressure of the sample. H_2SO_4 was dehydrated before experiments by passing Ar over the heated sample for more than 25 h. Because the presence of a small amount of H_2SO_4 does not affect the photochemistry of SO_3, we found that it is convenient to employ the aforementioned method to prepare matrix-isolated SO_3. Typically 10 mmol of gaseous mixture were deposited onto the cold target over a period 2–3 h. Proper dilution to suppress formation of aggregates was achieved by control of the temperature of the sample trap. The concentration ratios of SO_3:H_2SO_4:Ar were not determined, but we examined IR absorption spectra of SO_3 and H_2SO_4 to ensure that by proper dilution we avoided formation of dimers.

An ArF excimer laser (193 nm), operated at 10 Hz with

[a)]Corresponding author. Jointly appointed by the Institute of Atomic and Molecular Sciences, Academia Sinica, Taiwan, Republic of China.

energy 2.0–4.0 mJ/pulse, was employed to photodissociate the matrix sample. A KrF excimer laser (248 nm, 10 Hz, with energy 5–20 mJ/pulse) was subsequently employed for further dissociation to differentiate IR absorption lines of various photoproducts. IR absorption spectra were recorded at each stage of photolysis with a Fourier-transform infrared (FTIR) spectrometer equipped with a KBr beamsplitter and a Hg/Cd/Te detector cooled with liquid N_2 to cover the spectral range 500–4000 cm^{-1}. Typically 400 scans were collected at a resolution 0.5 cm^{-1}. $H_2{}^{34}SO_4$ (listed isotopic purity 90%) and $H_2S^{18}O_4$ (listed isotopic purity 82%) were obtained from ICON Service Inc.

III. COMPUTATIONAL DETAILS

The energies, vibrational frequencies, and equilibrium structures were calculated with GAUSSIAN94 program.[22] Because of the partial diradical character in OSOO, calculations at the MP2 level failed to provide reasonable vibrational frequencies. Hence, both methods used to optimize the geometries and to calculate the energies involve density functionals, described as (1) B3-LYP, a variation of Becke's three-parameter (local, nonlocal, Hartree–Fock) hybrid exchange functional using the Lee–Yang–Parr correlation functional,[23,24] and (2) B-P86, a method using Becke's exchange functional with Perdew's 1986 gradient-corrected correlation functional.[25,26] Relative energies of five possible isomers were calculated by two additional methods, the coupled cluster singles and doubles (CCSD) (Ref. 27) and CCSD(T) (Ref. 28), in which T stands for noniterative triple excitations, for geometries optimized at the B-P86 level. Dunning's correlation-consistent polarized valence triplet-zeta (cc-PVTZ) (Ref. 29) basis set was used at B-P86, CCSD, and CCSD(T) levels, whereas the basis augmented with s, p, d, and f functions (aug-cc-PVTZ) (Ref. 30) was used for the B3-LYP method. Analytic first derivatives were utilized in geometry optimization, and vibrational frequencies were calculated analytically at each stationary point for the B3-LYP and B-P86 methods.

IV. RESULTS AND DISCUSSION

The matrix samples contained SO_3 with minor H_2SO_4 impurity. The latter is inactive to photolysis at $\lambda \geqslant 193$ nm; irradiation of H_2SO_4 in solid Ar with a medium-pressure Hg lamp or laser emission at 193, 248, or 308 nm produced no change detectable with our infrared spectrometer. The species were well diluted so that nearly all guest compounds were in monomeric form. Hence, the presence of H_2SO_4 did not interfere in our investigation of photolysis of SO_3.

A. Infrared absorption of SO_3

Trace *A* of Fig. 1 shows absorption spectrum of SO_3 in solid Ar; lines observed at 2438.7, 1385.2, 527.1, and 490.3 cm^{-1} agree well with those reported previously at 2439.2, 1385.9, 527.6, and 489.9 cm^{-1}.[14] These lines are assigned as $\nu_1(a_1') + \nu_3(e')$, $\nu_3(e')$, $\nu_4(e')$, and $\nu_2(a_2')$, respectively; the symbols in parentheses indicate the symmetry class of the vibrational mode. The corresponding lines of various isotopic species of SO_3 are listed in Table I. Vibrational assignments based on these isotopic shifts are consistent with those reported in the gas phase. For example, the spectrum of a sample mixture of $S^{16}O_x{}^{18}O_{3-x}$ ($x=0$–3) with an overall atomic ratio ^{16}O:$^{18}O \simeq 1$:1 shows a quartet structure for ν_2 (at 490.3, 486.7, 483.0, and 479.4 cm^{-1}) with intensity ratios approximately 1:3:3:1, indicating a vibrational motion involving three equivalent O atoms. The pattern of isotopic shifts is consistent with the out-of-plane motion of SO_3. The e' symmetry of ν_3 and ν_4 degrades to C_{2v} when one or two ^{18}O atoms replace ^{16}O atoms in SO_3; consequently each line of $S^{16}O_x{}^{18}O_{3-x}$ ($x=1,2$) splits into two lines, consistent with

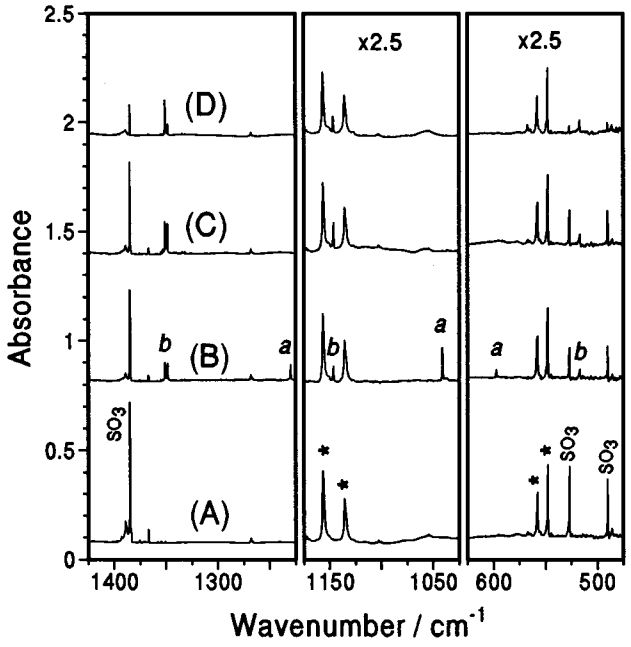

FIG. 1. IR absorption spectra of a SO_3/Ar matrix sample before and after irradiation. (*A*) Before irradiation; (*B*) after irradiation at 193 nm for 30 min; (*C*) further irradiation at 248 nm for 2 min; (*D*) another sample after irradiation at 248 nm for 40 min. Lines marked with an asterisk are H_2SO_4 impurities. Two sets of new lines after photolysis at 193 nm are labeled *a* and *b*. Traces are displaced vertically and the absorbance scale is expanded 2.5 times for wavenumbers smaller than 1200 cm^{-1} for ease of inspection.

TABLE I. IR absorption lines (in cm^{-1}) of various isotopic species of SO_3 in solid Ar.

Species	$\nu_1(a_1')+\nu_3(e')$	$\nu_3(e')$	$\nu_4(e')$	$\nu_2(a_2')$
$^{32}S^{16}O_3$	2438.7	1385.2	527.1	490.3
	(2443)[a]	(1391)	(529)	(495)
$^{18}O^{32}S^{16}O_2$	2417.3	[1385.2][b]	524.0	486.7
	2390.0	1358.6	513.4	
$^{16}O^{32}S^{18}O_2$	2385.4	1372.2	515.6	483.0
	2354.9	[1342.7][c]	504.7	
$^{32}S^{18}O_3$	2336.0	1342.7	501.6	479.4
$^{34}S^{16}O_3$	2420.4	1367.2	524.1	481.6

[a]Values for gaseous SO_3 are enclosed in parentheses.
[b]Line overlapped by the 1385.2 cm^{-1} line of $^{32}S^{16}O_3$.
[c]Line overlapped by the 1342.7 cm^{-1} line of $^{32}S^{18}O_3$.

our observation of six lines near 527 cm^{-1} (ν_4). A quartet rather than a sextet was observed for ν_3 near 1385 cm^{-1} because of line overlapping (Table I); an intensity ratio near 5:3:3:5 was observed for samples with overall atomic ratio ^{16}O:^{18}O=1:1.

B. Photolysis of SO_3

Irradiation of the matrix sample with laser emission at 193 nm for 30 min produced two sets of new lines, as illustrated in trace *B* of Fig. 1. Lines in set *A* (labeled "*a*" in Fig. 1) lie at 1229.6, 1041.3, and 597.6 cm^{-1}; these were not reported previously. Lines in set *B* (labeled "*b*" in Fig. 1) at 1351.1, 1348.1, 1147.0, and 517.3 cm^{-1} are readily identified as SO_2 by comparison with previous reports. Sodeau and Lee[17] reported two sites of SO_2 in solid Ar; SO_2 in the stable cubic close packing site absorbs at 1356.0, 1153.2, and 519.3 cm^{-1}, whereas SO_2 in the metastable hexagonal close packing site absorbs at 1352.2, 1148.5, and 517.7 cm^{-1}. Maillard *et al.*[31] reported two groups of absorption lines of SO_2 at (1355.0, 1352.8, 1152.2, and 519.5 cm^{-1}) and (1351.1, 1348.4, 1147.1, and 517.2 cm^{-1}) and assigned them to SO_2 in stable and metastable sites, respectively. Suzuki *et al.*[32] also observed lines corresponding to SO_2 in the metastable site. The lines in set *B* correspond well with those reported for SO_2 in a metastable site by Maillard *et al.*[31] Relatively weak lines at 1355.0, 1353.0, and 1151.0 cm^{-1} were also observed; they correspond to SO_2 in a stable site.

Further irradiation of the matrix sample with 248 nm laser emission for 2 min bleached lines in set *A*, as illustrated in trace *C* of Fig. 1. The intensities of lines in set *B* (due to SO_2) nearly doubled and those of SO_3 increased slightly. In a few experiments, the KrF excimer laser with emission at 248 nm was replaced by a low-pressure Hg lamp (at 253.7 nm), a XeCl laser (at 308 nm), or a dye laser (at 390 nm) pumped by a XeCl laser. In all cases, lines in set *A* disappeared readily whereas those of SO_3 increased; typically SO_3 increased more when a source at a greater wavelength was employed for secondary photolysis.

Photolysis of the SO_3/Ar matrix sample with laser emission at 248 nm produced only SO_2, as shown in trace *D* of Fig. 1 for an irradiation period of 40 min. Compared with the spectrum recorded after photolysis at 193 nm, the line at 1351.1 cm^{-1} is much more intense than that at 1348.1 cm^{-1}.

1. Isotopic shifts

Similar experiments with $^{34}SO_3$ and mixtures of $S^{16}O_x{}^{18}O_{3-x}$ (x=0–3) at varied proportions were performed. The observed lines in set *A* after photolysis at 193 nm are shown in Fig. 2; traces *A*–*C* were recorded after photolysis of matrix samples containing SO_3, $^{34}SO_3$, and a mixture of $S^{16}O_x{}^{18}O_{3-x}$ (x=0–3) with an overall atomic ratio ^{16}O:^{18}O≃1:1, respectively. The observed line positions of each isotopic species are listed in Table II.

Upon ^{34}S substitution, the line at 1229.6 cm^{-1} shifted to 1217.5 cm^{-1}, indicating that this vibrational mode involves motion of a sulfur atom. The $^{34}S/^{32}S$ isotopic ratio, 1217.5/1229.8=0.990, is identical to the theoretically predicted value for diatomic SO. Upon ^{18}O substitution with an overall

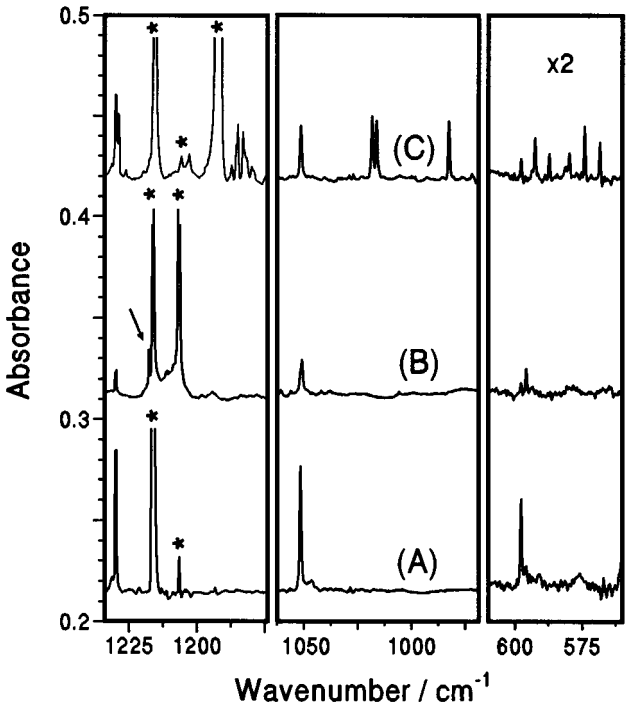

FIG. 2. IR absorption spectra of matrix samples after irradiation at 193 nm for 30 min. (*A*) SO_3/Ar matrix; (*B*) $^{34}SO_3$/Ar matrix; (*C*) Ar matrix containing $S^{16}O_x{}^{18}O_{3-x}$ (x=0–3) with an overall ratio ^{16}O:^{18}O≃1:1. Lines marked by an asterisk are due to various isotopic species of H_2SO_4 impurities. The arrow indicates one of the $O^{34}SOO$ line.

atomic ratio ^{16}O:^{18}O≃1:1, this line split into two groups of unresolved lines separated by approximately 45 cm^{-1}. The $^{18}O/^{16}O$ isotopic ratio, 1185.0/1229.6=0.964, agrees with that (0.962) predicted theoretically for diatomic SO. Therefore, the line at 1229.6 cm^{-1} is assigned to SO stretching. The wave number is greater than that of diatomic SO (1137 cm^{-1} in solid Ar) (Refs. 33 and 34) but near the average of symmetric and asymmetric stretching modes of SO_2 (~1250 cm^{-1}).

Upon ^{34}S substitution, the line at 1041.3 cm^{-1} shifted only 0.4 cm^{-1}, indicating little involvement of the motion of an S atom in this mode. Upon ^{18}O substitution, the line became a triplet with spacings ~27 cm^{-1}; the central member further split by 1.7 cm^{-1}. This pattern indicates the involve-

TABLE II. Observed vibrational wave numbers/cm^{-1} for various isotopic species of OSOO in solid Ar.

Species	SO-str.	OO-str.	SO-str./mixed bend
$^{16}O^{32}S^{16}O^{16}O$	1229.6	1041.3	597.6
$^{16}O^{32}S^{16}O^{18}O$	1229.6	1012.9	592.3
$^{16}O^{32}S^{18}O^{16}O$	1228.7	1014.6	579.6
$^{18}O^{32}S^{16}O^{16}O$	1185.0	1041.3	592.3
$^{16}O^{32}S^{18}O^{18}O$	1228.7	985.8	573.9
$^{18}O^{32}S^{16}O^{18}O$	1185.0	1012.9	587.0
$^{18}O^{32}S^{18}O^{16}O$	1183.0	1014.6	573.9
$^{18}O^{32}S^{18}O^{18}O$	1183.0	985.8	568.0
$^{16}O^{34}S^{16}O^{16}O$	1217.5	1040.9	595.6

ment of two nearly equivalent O atoms. The $^{18}O/^{16}O$ isotopic ratios, 1014.6/1041.3=0.974 and 1012.9/1041.3=0.973, are close to the predicted value 0.972 for diatomic $^{18}O^{16}O$. The $^{18}O/^{16}O$ isotopic ratio for the line with the smallest wave number in this group, 985.8/1041.3=0.947, is close to that (0.943) predicted for diatomic $^{18}O_2$. Therefore, this mode is assigned as OO stretching.

The line at 597.6 cm^{-1} is shifted to 595.6 cm^{-1} upon ^{34}S substitution. The $^{34}S/^{32}S$ isotopic ratio, 595.6/597.6=0.997 is slightly greater than the predicted ratio, 0.990, for diatomic SO. The $^{34}S/^{32}S$ isotopic ratio observed for OSO-bending of SO_2 is 513.0/517.3=0.992. Upon ^{18}O substitution with an overall atomic ratio $^{16}O:^{18}O \simeq 1:1$, this line became two triplets, each with intensity ratio approximately 1:2:1, indicating the involvement of three O atoms in this mode; the motions of two of them are similar but contribute less than the third one. The isotopic splittings are about 18, 6, and 5 cm^{-1} for substitution of the O atom at varied positions. The $^{18}O/^{16}O$ isotopic ratio of the major splitting, 579.6/597.6=0.970, is slightly greater than that predicted for diatomic SO (0.962). The $^{18}O/^{16}O$ isotopic ratios of the minor splittings, 592.3/597.6=0.991 and 587.0/597.6=0.982, are greater than that of the OSO bending mode of SO_2 (506.7/517.3=0.980). Hence, this mode is likely a mixed mode, possibly a combination of SO stretching, OSO bending, and SOO bending.

2. Assignments and mechanism of formation

Photolysis of SO_3 in the near ultraviolet was investigated by Norrish and Oldershaw[35] who proposed that the primary process is either

$$SO_3 \xrightarrow{h\nu} SO + O_2 \tag{4}$$

or

$$SO_3 \xrightarrow{h\nu} SO_2 + O. \tag{5}$$

Recently, Thelen and Huber[36] studied photodissociation of SO_3 at 193 nm by photofragmentation translational spectroscopy; they reported that reaction (5) with production of O atoms in the ^1D state is the primary channel, and a part of the hot SO_2 fragment undergoes secondary photodissociation to form SO and $O(^3P)$.

Lines in set *B* are identified as SO_2, whereas the absorption line of SO at 1137 cm^{-1} is undetectable. Hence, reaction (5) appears dominant during photolysis of SO_3 in solid Ar at 193 nm; secondary photolysis of hot SO_2 is probably unimportant in the cold matrix environment. Lines in set *A* correspond to no known absorptions of S_xO_y species. For example, SO_4 absorbs at 1434, 1267, 925, 777, 611, 498, and 490 cm^{-1}, and poly (sulfur oxide) absorbs at 1210, 1065, and 775 cm^{-1}.[16] The ^{34}S- and ^{18}O-isotopic experiments indicate that the species contains at least one S atom and three O atoms, and that the species possesses one S–O bond, one O–O bond, and very likely a second, much weaker, S–O bond. As the experiment was designed to produce isomers of SO_3 by means of the matrix cage effect, a likely candidate for the observed new photoproduct is OSOO or SOOO.

The possibility that the photoproduct is straight-chain SOOO is precluded for the following reasons. (1) The wave number (1229.6 cm^{-1}) of the SO-stretching mode is relatively large, indicating that the bonding is preferably described as a double bond. (2) The ^{18}O-isotopic shifts of the OO-stretching mode at 1041.3 cm^{-1} indicate a negligibly small contribution of the third O atom to this mode, contrary to what is expected for the structure of SOOO; variation of the mass of the third O atom in SOOO would generate a nonnegligible shift for the OO-stretching mode. (3) ^{34}S- and ^{18}O-isotopic shifts for the line at 597.6 cm^{-1} indicate a mode containing a weak SO-stretching mode mixed with other bending modes; the structure of SOOO is inconsistent with observation of such a mode. (4) Further photolysis of this product with laser emission at 248 nm produces SO_2 and SO_3; there is no simple mechanism for such photoprocesses from SOOO. (5) If SOOO were formed via the cage effect, a likely photolysis path would be reaction (4), but we detected no SO after photolysis of SO_3 at 193 nm. Similarly, the possibility of formation of a *cyclic*-SOOO is eliminated according to results from isotopic experiments.

The assignment of observed lines in set *A* to S-oxide–cyclic-SO_2, a three-membered ring compound shown as isomer I in Fig. 3, is not favored for the following reasons. (1) One expects two equivalent O atoms in structure I, but the ^{18}O-isotope experiment indicates that two O atoms involved in the OO-stretch differ slightly. (2) The wave number of the OO-stretching mode in a three-membered ring is expected to be smaller than that of an ordinary O–O bond; the observed line at 1041.3 cm^{-1} fits well with a typical peroxide bond, for example, 1101 cm^{-1} for HO_2,[37] 1112 cm^{-1} for CH_3O_2,[38] and 1052.3 cm^{-1} for HOOPO.[39] (3) The intensity of the SO stretch is expected to be much greater than that of the OO stretch in structure I because of its molecular symmetry. However, the observed intensities for lines at 1229.6 and 1041.3 cm^{-1} are similar.

Assignment of the newly observed lines in set *A* to OSOO is consistent with present experimental results. The wave number of the SO-stretching mode (1229.6 cm^{-1}) is near the average of symmetric and asymmetric stretches of SO_2, indicating a S–O bond similar to that of SO_2. The observed pattern of an OO-stretching mode for species with varied $^{18}O/^{16}O$ proportions is what one expects for OSOO; motions of two adjacent O atoms differ slightly because of the adjacent S atom, and motion of the third O atom has a negligible effect on this vibration because it is separated by the S atom from the OO moiety. As the central S–O bond is relatively weak, it is likely to couple with other bending modes; the observed isotopic shifts are consistent with a weak SO-stretching mode mixed with OSO-bending and SOO-bending modes.

Formation of OSOO may result from reactions in a matrix cage:

$$SO + O_2 \rightarrow OSOO \tag{6a}$$

$$\rightarrow SOOO \text{ and other products} \tag{6b}$$

or

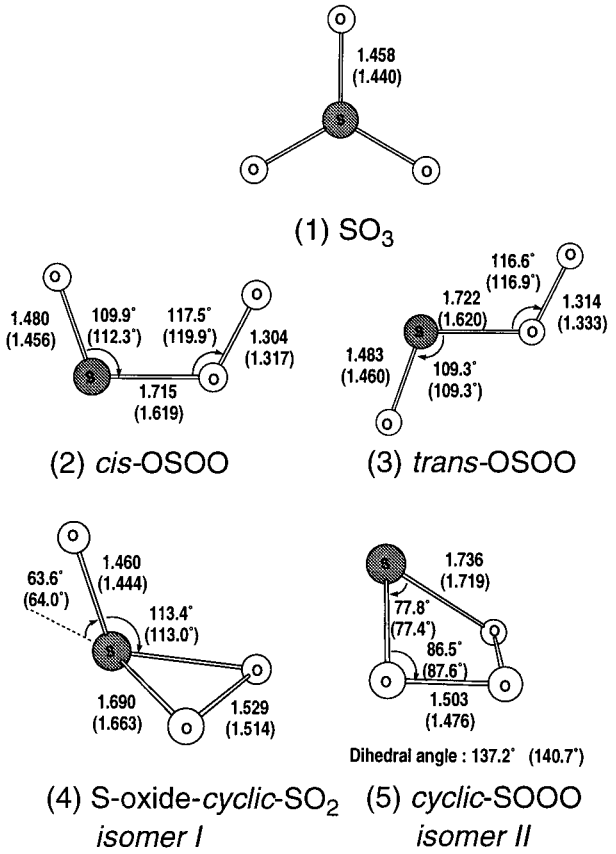

FIG. 3. Geometries of isomers of SO_3 calculated at the B-P86 level. Bond lengths are in units of Å; results obtained from the B3-LYP level are indicated in parentheses. The dihedral angle of isomer II is that between planes OSO and OOO.

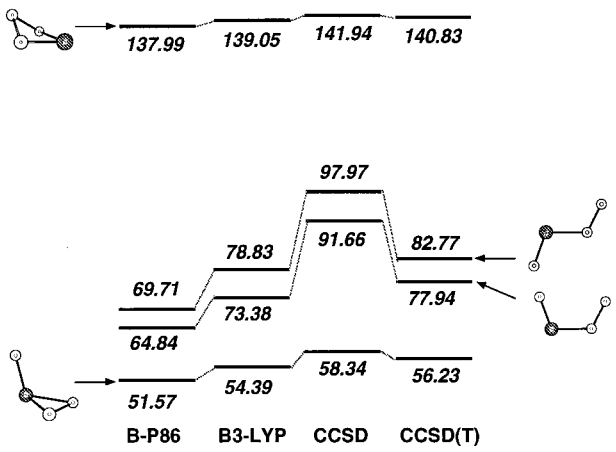

FIG. 4. Energies (in kcal mol^{-1}) of various isomers of SO_3 relative to that of SO_3 predicted at different levels of calculations. The energies of SO_3 at various levels of calculations are B-P86, −623.96855; B3-LYP, −623.92433; CCSD, −623.01603; CCSD (T), −623.06181 hartrees.

$$SO_2 + O \rightarrow OSOO \tag{7a}$$

$$\rightarrow SO_3 \text{ and other products.} \tag{7b}$$

However, detection of SO_2 (and OSOO) rather than SO after initial photolysis of SO_3, and detection of only SO_2 and SO_3 after secondary photolysis of OSOO, indicate that reactions (5) and (7a) are responsible for the formation of OSOO. We conclude that photolysis of SO_3 in solid Ar at 193 nm produces SO_2 and O; recombination of these photofragments in a matrix cage forms OSOO which absorbs at 1229.6, 1041.3, and 597.6 cm^{-1}.

There may be various stable conformers of OSOO, but we observed only one set of lines in our experiments. Irradiation of the matrix sample with the hydrogen Lyman-α line (121 nm) also produced the same set of lines of OSOO. Our experimental data provide no definitive information to assign conformation. If OSOO is formed via reactions (5) and (7a), formation of a *trans* isomer requires less geometric rearrangement than that of a *cis* isomer. However, in our experiments on photolysis of HNO_3 to form *cis–cis* and *trans-perp* HOONO, we found that the photolytic behavior of the products played an important role to determine the apparent quantum yield of each species.[18–21] If the photoproduct absorbs (and photodissociates) strongly at the same wavelength of photolysis, it may accumulate insufficient concentration to be detected.

Irradiation of the matrix sample with 248 nm laser emission produced only SO_2. Although it is possible that at 248 nm the photofragments may lack excess energy to overcome the barrier to form OSOO, it is more likely that OSOO is absent because it photodissociates readily at 248 nm, as observed in experiments of secondary photolysis. The formation of SO_2 rather than SO after photolysis of OSOO indicates that the O–O bond of OSOO dissociates at 248 nm.

V. COMPARISON WITH THEORETICAL CALCULATIONS

According to theoretical calculations, there are five stationary isomers of SO_3, as illustrated in Fig. 3; the geometries predicted for each isomer at both B-P86 and B3-LYP levels are also indicated, with results from the latter method listed in parentheses. The chain isomers (*cis*-OSOO and *trans*-OSOO) are planar whereas the ring isomers (I and II) are nonplanar. As expected, the O–O bonds (~1.52 Å) of ring isomers are much longer than those of chain isomers (~1.31 Å). Two types of S–O bonds in these isomers were predicted; the bonds in the ring structure and the central bonds in OSOO (1.69–1.74 Å) are much longer than those at terminal positions (1.46–1.48 Å). The central S–O bonds in *cis*- and *trans*-OSOO predicted by the B3-LYP method (~1.62 Å) are slightly shorter than those predicted by the B-P86 method (~1.72 Å).

Figure 4 shows energies of these isomers relative to that of SO_3 from calculations at various levels; the relative orders in energy are similar in all calculations. Relative to SO_3, ring isomer I has the least energy whereas ring isomer II has the greatest. *Cis*-OSOO lies approximately 5 kcal mol^{-1} below *trans*-OSOO. The energies of *cis*- and *trans*-OSOO at the CCSD(T) level decreased from those at the CCSD level by

TABLE III. Calculated vibrational wave numbers/cm^{-1}, infrared intensities, and $^{18}O/^{16}O$ isotopic ratios of SO_3.

	$\nu_1(a_1')$	$\nu_2(a_2')$	$\nu_3(e')$	$\nu_4(e')$
		B-P86/cc-PVTZ		
$S^{16}O_3$	992 (0.0)[a]	449 (24.3)	1310 (157)	483 (21.3)
		⟨$^{18}O/^{16}O$ isotropic ratios⟩		
$^{18}OS^{16}O_2$	0.979 [0.979][b,c]	0.993 [0.993][b]	1.000	0.994 [0.994][b]
			0.980 [0.981][b]	0.974 [0.974]
$^{16}OS^{18}O_2$	0.960 [0.961]	0.985 [0.985]	0.991 [0.991]	0.978 [0.978]
			0.969	0.957 [0.958]
$S^{18}O_3$	0.943 [0.943]	0.977 [0.978]	0.969 [0.969]	0.951 [0.952]
		B3-LYP/aug-cc-PVTZ		
$S^{16}O_3$	1045 (0.0)[a]	475 (32.1)	1364 (190)	508 (25.5)
		⟨$^{18}O/^{16}O$ isotopic ratios⟩		
$^{18}OS^{16}O_2$	0.979	0.993	1.000	0.994
			0.981	0.974
$^{16}OS^{18}O_2$	0.960	0.985	0.991	0.978
			0.969	0.957
$S^{18}O_3$	0.943	0.977	0.969	0.951

[a]Predicted infrared intensities (in km mol^{-1}) of $S^{16}O_3$ are listed in parentheses.
[b]Numbers in square brackets are experimental values from this work.
[c]Derived by subtracting wave numbers of ν_3 from that of $\nu_1+\nu_3$ in Table I.

approximately 15 kcal mol^{-1}, indicating that the noniterative triple excitations play important roles in this system.

Vibrational wave numbers, infrared intensities, and $^{18}O/^{16}O$ isotopic ratios of vibrational wavenumbers of SO_3 were calculated by the B-P86 and the B3-LYP methods, as listed in Table III. Unscaled results by the B3-LYP method underestimate vibrational wavenumbers of SO_3 by 1.6–3.8 %, whereas those at the B-P86 level differ by 5.7–9.2 %. The magnitudes of deviations provide a rough indication of possible errors in predictions of vibrational wave numbers of other isomers of SO_3. The predicted $^{18}O/^{16}O$ isotopic ratios agree well with experiments; the agreement is consistent with our previous experience[19,20] that even when predicted vibrational wave numbers deviate from experimental results by a relatively large fraction, predicted isotopic ratios typically show negligible errors.

Vibrational wave numbers predicted for two ring compounds (isomers I and II in Fig. 3) are listed in Table IV; they are listed in descending orders of wave numbers irrespective of corresponding symmetries. The four-membered *cyclic*-SOOO (isomer II) has vibrational wave numbers smaller than 900 cm^{-1} for all modes, as expected from its predicted geometry. Furthermore, predicted IR intensities are greatest for modes near 600 cm^{-1}. Hence, the possibility that observed new lines in set *A* are due to this isomer is clearly excluded. The three greatest vibrational wave numbers predicted for isomer I with a three-membered ring structure deviate from experimental observation by 0.8%, −9.8%, and 9.6% at the B-P86 level, and by 4.8%, −5.9%, and 15.0% at the B3-LYP level; the deviations much exceed those of typical calculations at such levels. Predicted relative IR intensities are also inconsistent with experimental observation. Therefore, it is unlikely that observed lines in set *A* are due to isomer I.

Vibrational wave numbers, infrared intensities, and $^{18}O/^{16}O$ isotopic ratios predicted for *cis*-OSOO and *trans*-OSOO are listed in Tables V and VI, respectively. The three greatest wave numbers predicted for both conformers are similar. Calculated values for SO-stretching and OO-stretching modes for both conformers deviate from line positions observed experimentally by less than 5% by both B-P86 and B3-LYP methods. However, the B-P86 method

TABLE IV. Calculated vibrational wave numbers/cm^{-1} and infrared intensities of ring isomers of SO_3.

	ν_1	ν_2	ν_3	ν_4	ν_5	ν_6
			B-P86/cc-PVTZ			
S-oxide–cyclic-SO_2	1239	939	655	580	414	318
(isomer I)	(149)[a]	(30.1)	(55.7)	(22.2)	(13.3)	(3.4)
cyclic-SOOO	840	709	698	584	564	349
(isomer II)	(2.4)[a]	(4.5)	(1.9)	(15.9)	(17.3)	(2.0)
			B3-LYP/aug-c-PVTZ			
S-oxide–cyclic-SO_2	1289	980	687	600	443	339
(isomer I)	(184)[a]	(39.2)	(60.5)	(22.3)	(16.4)	(4.3)
cyclic-SOOO	894	825	787	644	602	340
(isomer II)	(1.1)[a]	(0.5)	(11.3)	(15.0)	(22.0)	(2.0)

[a]Predicted infrared intensities (in km mol^{-1}) are listed in parentheses.

TABLE V. Calculated vibrational wave numbers/cm^{-1}, infrared intensities, and $^{18}O/^{16}O$ isotopic ratios of *cis*-OSOO.

	SO-str	OO-str	SO-str+mixed bend	Mixed bend	Out-of-plane	Mixed bend
			B-P86/cc-PVTZ			
cis-$^{16}OS^{16}O^{16}O$	1188(43.4)[a]	1088(118)	605(18.0)	446(5.6)	360(3.4)	162(1.5)
			$\langle^{18}O/^{16}O$ isotopic ratios$\rangle$			
$^{16}OS^{16}O^{18}O$	0.999[0.999][b]	0.972[0.973]	0.989[0.991]	0.996	0.989	0.975
$^{16}OS^{18}O^{16}O$	0.998[0.999]	0.975[0.974]	0.971[0.970]	0.974	0.973	0.999
$^{18}OS^{16}O^{16}O$	0.966[0.964]	0.997[0.999]	0.992[0.991]	0.999	0.992	0.970
$^{16}OS^{18}O^{18}O$	0.998[0.999]	0.945[0.947]	0.959[0.960]	0.971	0.962	0.974
$^{18}OS^{16}O^{18}O$	0.963[0.964]	0.971[0.973]	0.980[0.982]	0.995	0.982	0.946
$^{18}OS^{18}O^{16}O$	0.963[0.962]	0.973[0.974]	0.962[0.960]	0.973	0.965	0.970
$^{18}OS^{18}O^{18}O$	0.962[0.962]	0.945[0.947]	0.951[0.950]	0.970	0.954	0.945
			B3-LYP/aug-cc-PVTZ			
cis-$^{16}OS^{16}O^{16}O$	1250(95.5)[a]	1023(179)	654(25.0)	593(3.2)	383(5.1)	205(2.3)
			$\langle^{18}O/^{16}O$ isotopic ratios$\rangle$			
$^{16}OS^{16}O^{18}O$	1.000	0.971	0.999	0.988	0.990	0.973
$^{16}OS^{18}O^{16}O$	0.999	0.975	0.955	0.989	0.972	0.999
$^{18}OS^{16}O^{16}O$	0.964	1.000	0.995	0.994	0.993	0.972
$^{16}OS^{18}O^{18}O$	0.999	0.944	0.954	0.978	0.962	0.972
$^{18}OS^{16}O^{18}O$	0.963	0.971	0.994	0.982	0.983	0.946
$^{18}OS^{18}O^{16}O$	0.963	0.974	0.951	0.983	0.965	0.971
$^{18}OS^{18}O^{18}O$	0.963	0.944	0.950	0.971	0.955	0.944

[a]Predicted infrared intensities (in km mol^{-1}) of *cis*-$^{16}OS^{16}O^{16}O$ are listed in parentheses.
[b]Numbers in square brackets are experimental values from this work.

describes the mode near 600 cm^{-1} better, with wave numbers predicted for *cis*- and *trans*-OSOO deviate 1.2% and 3.1% from the observed value, respectively, as compared with deviations 9.4% and 17% derived at the B3-LYP method. Differences in wave numbers between *cis*- and *trans*-OSOO are distinct only for modes below 450 cm^{-1}, beyond our detection limits; therefore we cannot determine the conformation of observed photoproducts on the basis of observed vibrational wave numbers. ^{18}O-isotopic shifts of both SO-stretching and OO-stretching modes are also similar for both conformers, as listed in Tables V and VI, but a distinct difference is predicted for the mode near 600 cm^{-1}. When the terminal ^{16}O atom adjacent to the S atom is substituted with an ^{18}O atom, *cis*-OSOO shows greater isotopic shifts than *trans*-OSOO. For example, the isotopic ratios are 0.980 and 0.989 for *cis*- and *trans*- $^{18}OS^{16}O^{18}O$, respectively, by the B-P86 method; the difference is greater than typical errors (<0.003) expected for calculations at such a level.

TABLE VI. Calculated vibrational wave numbers/cm^{-1}, infrared intensities, and $^{18}O/^{16}O$ isotopic ratios of *trans*-OSOO.

	SO-str	OO-str	SO-str+mixed bend	Mixed bend	Mixed bend	Out-of-plane
			B-P86/cc-PVTZ			
trans-$^{16}OS^{16}O^{16}O$	1170 (87.6)[a]	1070 (185)	616(13.5)	346(4.3)[a]	210(12.0)	203(4.6)
			$\langle^{18}O/^{16}O$ isotopic ratios$\rangle$			
$^{16}OS^{16}O^{18}O$	1.000[0.999][b]	0.972[0.973]	0.992[0.991]	0.985	0.984	0.983
$^{16}OS^{18}O^{16}O$	1.000[0.999]	0.974[0.974]	0.969[0.970]	0.980	0.993	0.979
$^{18}OS^{16}O^{16}O$	0.964[0.964]	0.999[0.999]	0.997[0.991]	0.988	0.981	0.987
$^{16}OS^{18}O^{18}O$	0.999[0.999]	0.944[0.947]	0.961[0.960]	0.966	0.977	0.961
$^{18}OS^{16}O^{18}O$	0.963[0.964]	0.971[0.973]	0.989[0.982]	0.972	0.966	0.970
$^{18}OS^{18}O^{16}O$	0.963[0.962]	0.974[0.974]	0.965[0.960]	0.968	0.974	0.966
$^{18}OS^{18}O^{18}O$	0.963[0.962]	0.944[0.977]	0.957[0.950]	0.954	0.958	0.948
			B3-LYP/aug-cc-PVTZ			
trans-$^{16}OS^{16}O^{16}O$	1235(153)[a]	1001(190)[a]	700(38.8)[a]	445(3.6)[a]	252(14.5)	205(6.2)[a]
			$\langle^{18}O/^{16}O$ isotopic ratios$\rangle$			
$^{16}OS^{16}O^{18}O$	1.000	0.973	0.996	0.982	0.982	0.983
$^{16}OS^{18}O^{16}O$	1.000	0.974	0.964	0.985	0.991	0.979
$^{18}OS^{16}O^{16}O$	0.963	1.000	0.999	0.983	0.984	0.987
$^{16}OS^{18}O^{18}O$	1.000	0.946	0.960	0.969	0.973	0.962
$^{18}OS^{16}O^{18}O$	0.963	0.973	0.995	0.964	0.966	0.970
$^{18}OS^{18}O^{16}O$	0.963	0.974	0.963	0.968	0.975	0.965
$^{18}OS^{18}O^{18}O$	0.963	0.946	0.959	0.952	0.958	0.948

[a]Predicted infrared intensities (in km mol^{-1}) of *trans*-$^{16}OS^{16}O^{16}O$ are listed in parentheses.
[b]Numbers in square brackets are experimental values from this work.

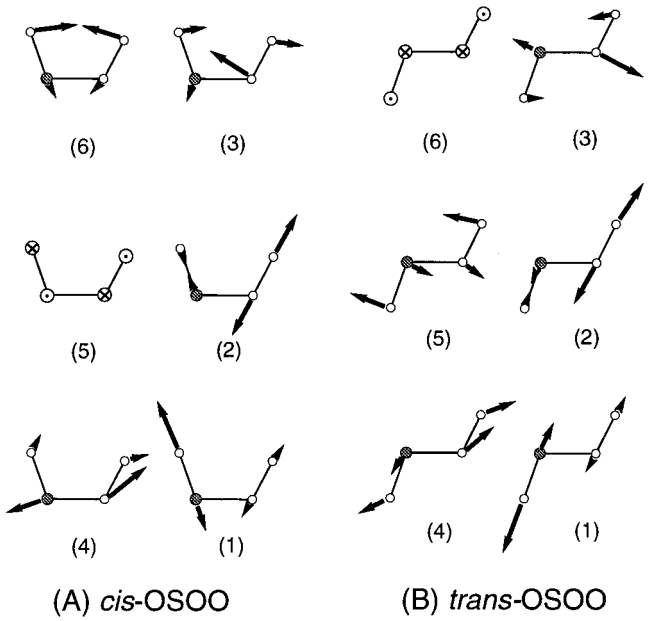

FIG. 5. Vibrational modes of *cis*-OSOO and *trans*-OSOO calculated at the B-P86 level. The modes are ordered in descending wave numbers.

$^{18}O/^{16}O$ isotopic ratios observed for these three modes fit well (within 0.002) with those predicted for *cis*-OSOO, whereas they differ by as much as 0.007 from those predicted for *trans*-OSOO. Hence, we conclude that observed lines in set *A* at 1229.6, 1041.3, and 597.6 cm^{-1} are likely due to *cis*-OSOO.

The six vibrational modes of *cis*-OSOO and *trans*-OSOO predicted by the B-P86 method are shown in Fig. 5. The two modes with greatest energies are mainly SO stretch and OO stretch, consistent with observed isotopic shifts. The mode near 600 cm^{-1} for *cis*-OSOO corresponds to motions of stretching of the central S–O bond mixed with OSO and SOO bending; the motions of two terminal O atoms are nearly equivalent, thus yielding nearly identical vibrational wave numbers for $^{16}OS^{16}O^{18}O$ and $^{18}OS^{16}O^{16}O$, and for $^{16}OS^{18}O^{18}O$ and $^{18}OS^{18}O^{16}O$. This pattern is exactly what we observed in the line splitting after photolysis of a mixture of $S^{16}O_x{}^{18}O_{3-x}$ ($x=0$–3). The corresponding mode for *trans*-OSOO involves less motion of the terminal O atom adjacent to the S atom, hence $^{18}O/^{16}O$ isotopic ratios are predicted to be greater than those of *cis*-OSOO as the terminal ^{16}O atom adjacent to the S atom is substituted with an ^{18}O atom.

As described previously, the major difference in geometries predicted for *cis*- and *trans*-OSOO between the B-P86 and the B3-LYP methods is that the lengths of the central S–O bond are predicted to be approximately 0.1 Å greater than those predicted at the B3-LYP level. Consequently, the corresponding frequencies and isotopic shifts of the vibrational mode near 600 cm^{-1} are better described at the B-P86 level. In order to eliminate the possibility that the inadequacy in prediction at the B3-LYP level is due to insufficient basis set, we used the aug-cc-PVTZ basis set for B3-LYP computations; the results show no improvement on the description of the mode near 600 cm^{-1}.

VI. CONCLUSION

We photolyzed SO_3 in solid Ar with an ArF excimer laser at 193 nm and observed IR absorption lines at 1229.6, 1041.3, and 597.6 cm^{-1} due to OSOO, likely in a *cis* conformation. Vibrational assignments were based on ^{18}O- and ^{34}S-isotopic shifts. The results are consistent with theoretical calculations. Our experimental results indicate that photolysis of SO_3 at 193 nm yields $O+SO_2$ which recombine in the matrix cage to form OSOO. This observation is the first of such an isomer of SO_3.

ACKNOWLEDGMENT

We thank the National Science Council of the Republic of China for support of this research (Contract No. NSC84-2113-M-007-012).

[1] R. P. Wayne, *The Chemistry of the Atmosphere*, 2nd ed. (Clarendon, Oxford, 1991).
[2] J. C. Calvert, A. Lazarus, G. L. Kok, B. G. Heikes, J. G. Walega, J. Lind, and C. A. Cantrell, Nature **317**, 27 (1985).
[3] L. Langner, H. Rodhe, P. J. Crutzen, and P. Zimmerman, Nature **359**, 712 (1992), and references therein.
[4] S. Solomon, Nature **347**, 347 (1990), and references therein.
[5] W. R. Stockwell and J. G. Calvert, Atmos. Environ. **17**, 2231 (1983).
[6] *SO_2, NO and NO_2 Oxidation Mechanisms: Atmospheric Considerations*, Acid Precipitation Series, Vol. 3, edited by J. G. Calvert (J. I. Teasley, Series Editor) (Butterworth, Boston, 1984).
[7] K. R. Leopold, K. H. Bowen, and W. Klemperer, J. Chem. Phys. **74**, 4211 (1981).
[8] R. Bent and W. R. Ladner, Spectrochim. Acta **19**, 931 (1963).
[9] A. J. Dorney, A. R. Hoy, and I. M. Mills, J. Mol. Spectrosc. **45**, 253 (1973).
[10] S. Y. Tang and C. W. Brown, J. Raman Spectrosc. **3**, 387 (1975).
[11] A. Kaldor, A. G. Maki, A. J. Dorney, and I. M. Mills, J. Mol. Spectrosc. **45**, 247 (1973).
[12] N. J. Brassington, H. G. M. Edwards, D. W. Farwell, D. A. Long, and H. R. Mansour, J. Raman Spectrosc. **7**, 154 (1978).
[13] N. F. Henfrey and B. A. Thrush, Chem. Phys. Lett. **102**, 135 (1983).
[14] V. E. Bondybey and J. H. English, J. Mol. Spectrosc. **109**, 221 (1985).
[15] A. G. Hopkins, S. Tang, and C. W. Brown, J. Am. Chem. Soc. **95**, 3486 (1973).
[16] R. Kugel and H. Taube, J. Phys. Chem. **79**, 2130 (1975).
[17] J. R. Sodeau and E. K. C. Lee, J. Phys. Chem. **84**, 3358 (1980).
[18] W.-J. Lo and Y.-P. Lee, J. Chem. Phys. **101**, 5494 (1994).
[19] W.-J. Lo, M.-y. Shen, C.-h. Yu, and Y.-P. Lee, J. Chem. Phys. **104**, 935 (1996).
[20] W.-J. Lo, Y.-P. Lee, J.-H. M. Tsai, H.-H. Tsai, T. P. Hamilton, J. G. Harrison, and J. S. Beckman, J. Chem. Phys. **103**, 4026 (1995).
[21] B.-M. Cheng, J.-W. Lee, and Y.-P. Lee, J. Phys. Chem. **95**, 2814 (1991).
[22] GAUSSIAN 94 (Revision B.2), M. J. Frisch, G. W. Trucks, H. B. Schlegel, P. M. W. Gill, B. G. Johnson, M. A. Robb, J. R. Cheeseman, T. A. Keith, G. A. Petersson, J. A. Montgomery, K. Raghavachari, M. A. Al-Laham, V. G. Zakrzewski, J. V. Ortiz, J. B. Foresman, J. Cioslowski, B. B. Stefanov, A. Nanayakkara, M. Challacombe, C. Y. Peng, P. Y. Ayala, W. Chen. M. W. Wong, J. L. Andres, E. S. Replogle, R. Gomperts, R. L. Martin, D. J. Fox, J. S. Binkley, D. J. Defrees, J. Baker, J. P. Stewart, M. Head-Gordon, C. Gonzalez, and J. A. Pople (Gaussian Inc., Pittsburgh, PA, 1995).
[23] A. D. Becke, J. Chem. Phys. **98**, 5648 (1993).
[24] C. Lee, W. Yang, and R. G. Parr, Phys. Rev. B **37**, 785 (1988).
[25] A. D. Becke, Phys. Rev. A **38**, 3098 (1988).
[26] J. P. Perdew, Phys. Rev. B **33**, 8822 (1986).
[27] G. D. Purvis and R. J. Bartlett, J. Chem. Phys. **76**, 1910 (1982); G. E. Scuseria, C. L. Janssen, H. F. Schaefer III, *ibid*. **89**, 7382 (1988).

[28] J. A. Pople, M. Head-Gordon, and K. Raghavachari, J. Chem. Phys. **87**, 5968 (1987).
[29] T. H. Dunning, Jr., J. Chem. Phys. **90**, 1007 (1989); D. E. Woon and T. H. Dunning, Jr., *ibid*. **98**, 1358 (1993).
[30] R. A. Kendall, T. H. Dunning, Jr., and R. J. Harrison, J. Chem. Phys. **96**, 6796 (1992).
[31] D. Maillard, M. Allavena, and J. P. Perchard, Spectrochim. Acta **31**A, 1523 (1975).
[32] E. M. Suzuki, J. W. Nibler, K. A. Oakes, and D. Eggers, J. Mol. Spectrosc. **58**, 201 (1975).
[33] A. G. Hopkins and C. W. Brown, J. Chem. Phys. **62**, 2511 (1975).
[34] C.-C. Zen, F.-T Tang, and Y.-P. Lee, J. Chem. Phys. **96**, 8054 (1992).
[35] R. G. W. Norrish and G. A. Oldershaw, Proc. R. Soc. London Sec. A **249**, 498 (1959).
[36] M.-A. Thelen and J. R. Huber, Chem. Phys. Lett. **236**, 558 (1995).
[37] M. E. Jacox, J. Phys. Chem. Ref. Data **19**, 1387 (1990).
[38] K. McAdam, B. Veyret, and R. Lesclaux, Chem. Phys. Lett. **133**, 39 (1987).
[39] R. Withnall and L. Andrews, J. Phys. Chem. **91**, 784 (1987).